PERGAMON

Electrochimica Acta 45 (1999) 225–233

ELECTROCHIMICA Acta

www.elsevier.nl/locate/electacta

Interfacial studies of a thin-film $Li_2Mn_4O_9$ electrode

Robert Kostecki*, Fanping Kong, Yoshiaki Matsuo, Frank McLarnon

Environmental Energy Technologies Division, Lawrence Berkeley National Laboratory, Berkeley, CA 94720, USA

Received 14 March 1999; received in revised form 9 May 1999

Abstract

A thin-film spinel $Li_2Mn_4O_9$ electrode was prepared by spin coating onto a Pt substrate. Spectroscopic ellipsometry, X-ray diffraction and current-sensing atomic force microscopy (CSAFM) were used to characterize interfacial processes and film formation at this electrode in the presence of 1.0 M $LiPF_6$, EC:DMC (1:1 by volume) electrolyte. Prolonged exposure of the film to the electrolyte at ambient temperature resulted in spontaneous decomposition of the spinel to λ-MnO_2 without disruption of the original structure. The surface of the resulting λ-MnO_2 film exhibited no significant change in morphology, however a thin passive electrode surface layer was detected by the CSAFM probe. This electrode surface layer exhibited insulating properties and most likely contained Li_2O, a by-product of $Li_2Mn_4O_9$ decomposition. Published by Elsevier Science Ltd.

Keywords: Interfacial films; Manganese oxide electrode

1. Introduction

Among the processes which are known to lead to capacity fade in lithium-ion cells, structural changes of the active material and passive film formation at the electrode and current collector surfaces are believed to contribute significantly to the overall degradation mechanism. The presence of a solid electrolyte interphase (SEI) passivation layer at the negative electrode (carbon)/electrolyte interface has been well documented in the literature [1–6]. A passive layer is formed primarily during early cycles because of irreversible side reactions that occur at the interface between the electrode and electrolyte. However, the composition and morphology of the SEI layer change continuously and play major roles in determining carbon electrode and battery calendar life, cycling efficiency and irreversible capacity loss.

Several studies of positive electrode passivation and dissolution phenomena have been reported in the literature, and most focus on the lithium manganese oxide spinel cation-dissolution process [7–10]. Dissolution of the $LiMn_2O_4$ active material may occur via a disproportionation mechanism due to the instability of the Mn^{3+} oxidation state, which reacts spontaneously to form Mn^{2+} and Mn^{4+}, leading to subsequent Mn deposition on the negative electrode [7,8,11,12]. Another dissolution mechanism is induced by acids that are generated as a result of the electrochemical oxidation of solvent molecules on composite cathodes, or acids that are generated by the reaction between F-containing anions and impurity water [8,11–14]. The Mn^{2+} dissolution reaction is also believed to occur in fully discharged $LiMn_2O_4$ electrodes and can substantially reduce the calendar life of discharged cells [7,8].

Recently Xia et al. [15] reported that the capacity loss caused by the simple dissolution of Mn^{3+} accounted for only 23 and 34% of the overall loss observed at room temperature and 50°C, respectively. They suggested that the transformation of an unstable

* Corresponding author.

0013-4686/99/$ - see front matter Published by Elsevier Science Ltd.
PII: S0013-4686(99)00206-6

two-phase structure into a more stable one-phase structure occurs via loss of MnO (a disproportionation mechanism) which dominates capacity fading during cell cycling at room temperature and 50°C. AC impedance measurements revealed that the capacity loss at high temperature was due in part to decomposition of the electrolyte solution at the electrode. This process is greatly accelerated at higher temperatures and results in the formation of an ionically conducting but electronically insulating surface layer.

Although the $LiPF_6$-EC/DMC electrolyte solution has been reported to be stable up to 4.9 V (vs Li/Li^+) at an $LiMn_2O_4$ electrode at room temperature [8], its stability remains in question during prolonged exposure to the electrolyte or cycling when the surface structure of the original material may undergo significant modification. In the presence of unstable oxide phases and point defects, surface morphology changes and cation dissolution/precipitation processes can lead to slow electrolyte decomposition and the formation of a thin electrode surface film. Changes in the physicochemical properties of the surface film, i.e. its thickness, homogeneity, electronic and ionic conductivity and solvent permeability, can contribute to the electrode resistance and thereby increase cell polarization, leading to incomplete charging and consequent capacity losses.

Pasquier et al. [16] very recently addressed the issue of chemical stability of high-surface-area $LiMn_2O_4$ in various Li-based electrolytes at elevated temperatures. They identified the growth of a protonated λ-MnO_2 phase upon storage of $LiMn_2O_4$ in the electrolyte at 100°C. Such a phase exhibits reduced capacity and contributes to irreversible capacity loss at high temperatures. Moreover, it was shown that upon aging at 100°C the $LiMn_2O_4$ particles are modified by the formation of a surface passivating layer that contains Li and Mn species which are soluble in water and decompose upon heating above 200°C with the release of CO_2.

Spectroscopic ellipsometry is particularly well suited to study surface and interfacial phenomena in electrochemical systems [17–20], because of its sensitivity and noninvasive nature. However, there are few quantitative ellipsometric studies of electrodes with porous or semiporous surfaces. This is because the severe depolarization effect which accompanies light beam reflection from a rough surface reduces the sensitivity of ellipsometric measurements, and because mathematical modeling of a rough electrode surface requires additional data-fitting parameters.

In this paper we examine interfacial phenomena at the surface of a thin-film lithiated manganese oxide electrode upon exposure to 1 M $LiPF_6$-EC/DMC (1:1 by volume) electrolyte at ambient temperature. The electrode contained a considerable number of point defects and significant crystal disorder, features which are expected to facilitate dissolution processes at the electrode/electrolyte interface. This thin-film electrode was also very suitable for surface studies by optical techniques. This material is clearly not appropriate for use as a battery electrode, however it is highly attractive for studies of interfacial phenomena.

We used spectroscopic ellipsometry, current-sensing atomic force microscopy (CSAFM), Raman spectroscopy, and X-ray diffraction to study the changes in electrode surface morphology, conductivity and optical constants which accompany lithium intercalation and deintercalation. Surface roughness parameters derived from statistical analyses of AFM images were used to help determine precise optical constants from ellipsometric data. Special emphasis was placed on characterizing electrode dissolution/phase transformation processes and the formation of surface layers at the metal oxide/electrolyte interface, with minimal electrochemical characterization because of the inherent long-term instability of the thin-film electrode.

2. Experimental

Lithium manganese oxide films were prepared by spin coating of a homogeneous precursor solution onto a Pt substrate. The precursor solution was prepared by a procedure similar to that proposed by Amine et al. [21]. Ethanolic solutions of manganese acetate tetrahydrate (0.32 M, 20 ml) and lithium nitrate (0.32 M, 10 ml) were mixed, the resultant solution was stirred for several minutes, and an excess amount of ammonium hydroxide (28%, 3 ml) was added. The solution color then changed to dark brown, indicating the formation of gelatinous $LiMn_2(OAc)_3(OH)_2$ particles [22]. The solid particles in this homogenous phase were spin-coated onto a Pt substrate at 900 rpm. The resulting gel precursor film was dried on a hot plate at 150°C for 5 min and then at 200°C for 5 min. The film was transformed into $LiMn_2O_4$ by heating at 260°C for 5 min. Because the film was very thin at this stage, the above described spin-coating procedure was repeated 10 times (except for the first heating at 150°C), and the resultant film was calcined at 260°C in air for 20 h.

Crystal structures of the $LiMn_2O_4$ thin films were determined using a Siemens Kristalloflex diffractometer with CuKα radiation. Ex situ Raman spectra were recorded using a Coherent Inc. Model Innova 70 argon-ion laser, $\lambda = 514.5$ nm, an HR320 Spectrograph (Instruments SA, Inc.), and am EG&G Multichannel Analyzer Model 1463. The power of the incident laser beam (0.1×3 mm) measured at the sample was 30 mW.

Ex situ CSAFM images were obtained with a

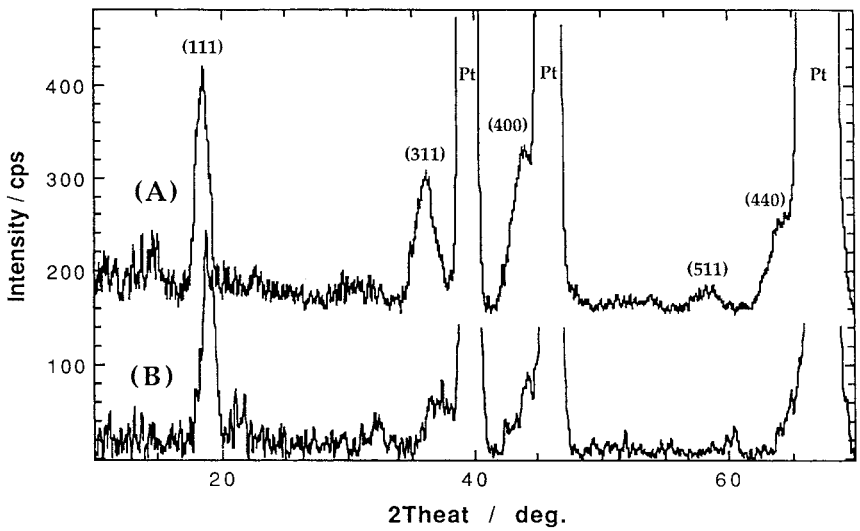

Fig. 1. X-ray diffraction pattern of a spin-coated lithium manganese oxide thin film. (A) freshly prepared film, (B) after 4 days exposure to 1.0 M $LiPF_6$ in EC/DMC electrolyte.

Molecular Imaging (MI) scanning probe microscope coupled with a Park Scientific Instruments (PSI) electronic controller. The CSAFM measurements were carried out in the constant-force mode, i.e. the piezoelectric scanner followed the surface profile of the sample and it adjusted itself to the changing thickness of the surface film. Platinum-coated Si microlevers (0.12 Nm^{-1}) were used to probe the local conductivity of the samples. Surface morphology imaging was carried out simultaneously with conductivity mapping of the $LiMn_2O_4$ electrode.

For our ellipsometry experiments, a 44-channel Woollam ellipsometer (M-44 system) and both WVASE32 (a Woollam program based on a Marquardt–Levenberg algorithm) and FlexiFit (a LBNL program based on a downhill simplex algorithm) data-fitting programs were used to determine the thin-film optical constants and to monitor electrode surface modifications upon exposure to the electrolyte. To achieve maximum sensitivity, a 75° incident angle was chosen (close to the Brewster angles of most solid/liquid interface systems). A long integration time was necessary to collect good quality ellipsometric spectra.

Electrochemical experiments were carried out in a two-electrode polypropylene cell. Metallic Li was used as counter and reference electrodes. The electrolyte was commercial 1.0 M $LiPF_6$ in EC/DMC (1:1 by volume) obtained from Grant Chemical Division, Farro Co. After prolonged exposure to the electrolyte, the thin-film electrodes were washed with DMC before being transferred under a He atmosphere into the ellipsometric cell and then into the CSAFM cell. Cyclic voltammetry (CV) measurements were carried out with a Model 362 EG&G scanning potentiostat.

3. Results and discussion

3.1. Characterization of lithium manganese oxide thin films

To assess the sample composition, elemental analyses for Li and Mn were carried out using inductively coupled plasma emission spectroscopy (ICPES). The calculated Mn:Li ratio was 2.0:0.95 (5% error margin) indicating slight a lithium deficiency. Such a lack of stoichiometry in a thermally synthesized lithium manganese oxide film may suggest the presence of impurities, most probably Mn_2O_3. Rutheford Backscattering Spectrometry (RBS) measurements were carried out to confirm the ICP data and also to determine the oxygen content. These measurements yielded a similar Mn:Li ratio, however the associated oxygen error was sufficiently large to preclude consideration as a true value.

Figure 1(A) shows the X-ray diffraction pattern of a freshly prepared lithium manganese oxide thin film on a Pt substrate after calcination at 260°C for 20 h. The signal intensity is low, however 4 diffraction peaks at $2\theta = 18.6°$, 36.4°, 44.3° and 63.9° which originate from the oxide thin film are clearly observed. Miller indices can be assigned to these peaks by assuming a cubic spinel structure with an Fd3m space symmetry group. The cubic cell lattice parameter was calculated to be

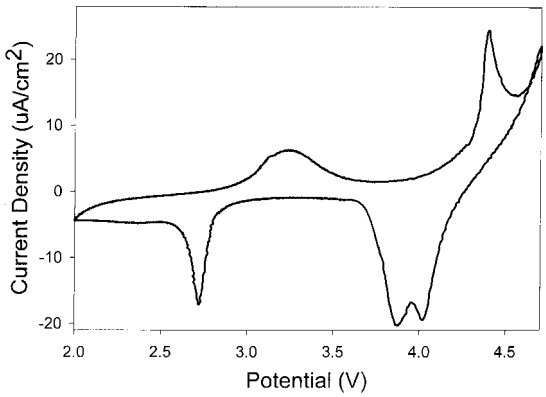

Fig. 2. Cyclic voltammogram of a freshly deposited thin film in 1.0 M $LiPF_6$ in EC/DMC at $v = 6$ mV/min.

$a = 0.819$ nm. This value is very similar to that obtained by Amine et al [21], suggesting that this sample was a spinel of stoichiometry close to $Li_2Mn_4O_9$. On the other hand, the apparent weakness of the X-ray signal suggests that the sample may contain a significant amount of an amorphous phase. Possible structural impurities which are incorporated in the film escaped detection because of their low concentration and/or amorphous character. Such oxygen rich poorly crystallized lithium manganese oxides are characteristic for a low temperature synthesis process.

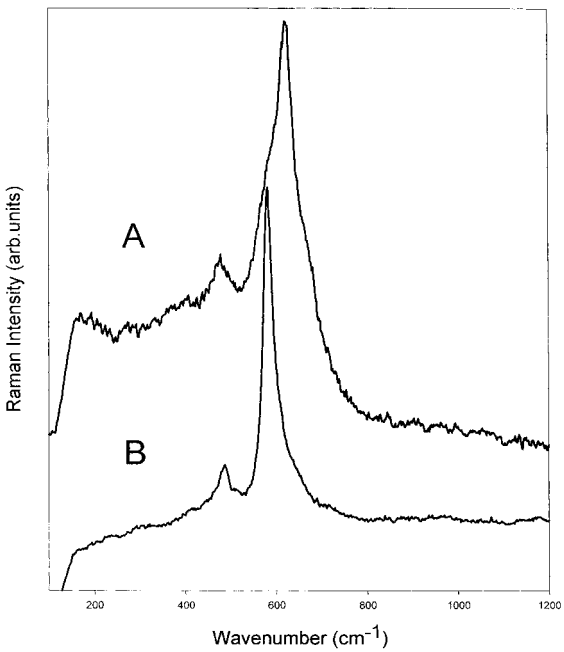

Fig. 3. Raman spectrum of a spin-coated lithium manganese oxide thin film. (A) freshly prepared film, (B) after 4 days exposure to 1.0 M $LiPF_6$ in EC/DMC electrolyte.

A CV curve for the film in 1.0 M $LiPF_6$ in EC/DMC (1:1 by volume) between 2.0 and 4.7 V is shown in Fig. 2. This CV originated at the initial open-circuit potential (ca. 3.65 V) with a negative going sweep. Two sets of peaks are visible, one centered around 3.0 V and one around 4.2 V. The anodic current due to the electrolyte decomposition becomes visible at potentials higher than 4.2 V. During the initial cathodic scan $Li+$ ions are inserted into the defect spinel structure to form the rock salt phase $Li_5Mn_4O_9$, and then during the anodic scan lithium extraction occurs in two stages which can be attributed to lithium removal from octahedral and tetrahedral sites [23]. The strong contribution from electrolyte decomposition at potentials above 4.2 V suggests the presence of a considerable amount of lattice defects which catalyze the electrolyte oxidation process.

The Raman spectrum of a freshly prepared thin film is shown in Fig. 3(A). The spectrum is dominated by a strong and broad peak at 620 cm^{-1}. This band is believed to consist of three separate bands at 580, 620 and 695 cm^{-1} which can be interpreted as contributions from Mn-O vibration modes within the spinel structure. Another medium-intensity band at 478 cm^{-1} can be assigned to the vibrations of distorted octahedral MnO_6 units. All of these bands lie on a large and broad maximum which extends from 150 to 900 cm^{-1}. This vibrational behavior of solid metal oxides usually involves contributions from a highly disordered or amorphous phase, which therefore must be present in our lithium manganese oxide film in considerable quantities. Although it is impossible to determine the exact stoichiometry of the film material from the Raman spectrum, these data support the conclusions derived from the X-ray spectrum.

Figure 4 shows topographic AFM (left) and CSAFM (right) images (5×5 μm and 1×1 μm areas) of the freshly deposited $Li_2Mn_4O_9$ thin film on a Pt substrate. The film morphology can be described as formations of small densely packed globular particles. A typical particle size was about 400 nm, however spaces between them were filled with smaller grains of irregular shape, resulting in a compact and relatively smooth surface. The average height and the average roughness of the film surface were 28.7 and 5.3 nm, respectively, i.e. quite smooth. The particle size was about 10 times smaller that of the powders used in the cathode fabrication process. The small roughness and good homogeneity of the film surface made it suitable for optical studies of interface processes.

Conductivity mapping was carried out at two different potential biases, 0.01 and 1.0 V. The shades of gray on these images represent the sample-to-tip cur-

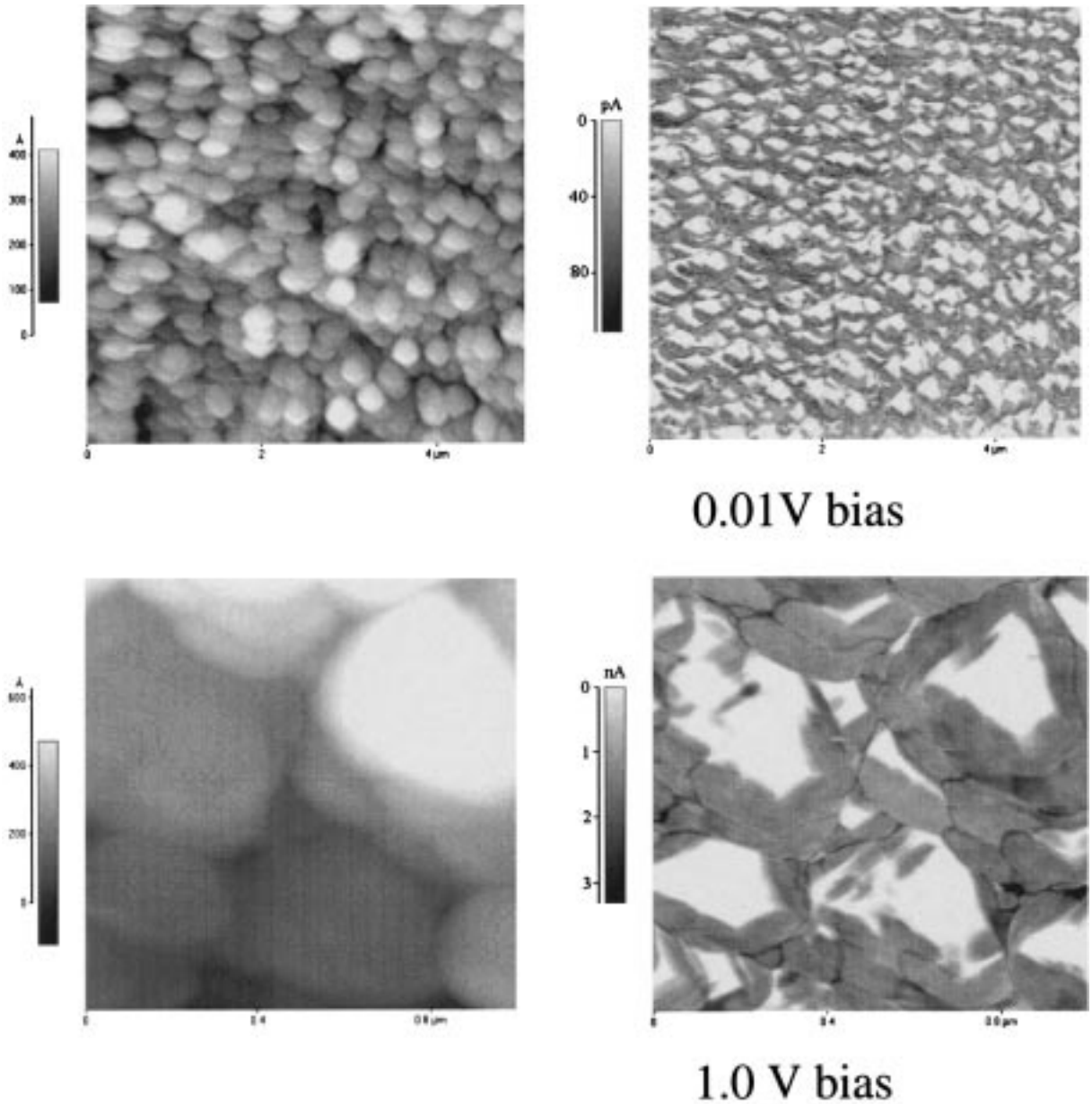

Fig. 4. CSAFM topographic (left) and conductivity (right) images of a freshly deposited $Li_2Mn_4O_9$ thin film on a Pt substrate.

rent value at the given sample-to-tip bias. Darker areas in the conductivity images are more conductive than brighter areas. Images recorded at 1.0 V bias showed better contrast and revealed a highly nonuniform (at the nanoscale) electronic conductivity of the thin film. Surprisingly, the conductivity varied substantially within the surface area of a single large grain. Characteristically, areas on the top of the grains exhibit very poor conductivity compared to the areas on the grain sides where the conductivity was substantially higher, albeit somewhat variable. Small particles located in the intergranular spaces showed rather uniform and good electronic conductivity. The surface topography itself may also have a small effect on the magnitude of current passing between the tip and the sample. Basically, this 'topography' current is a function of the tip profile and a changing surface geometry which determines the contact area between them. This interaction reveals the boundaries between grains as dark, sharp and thin lines, however this effect cannot

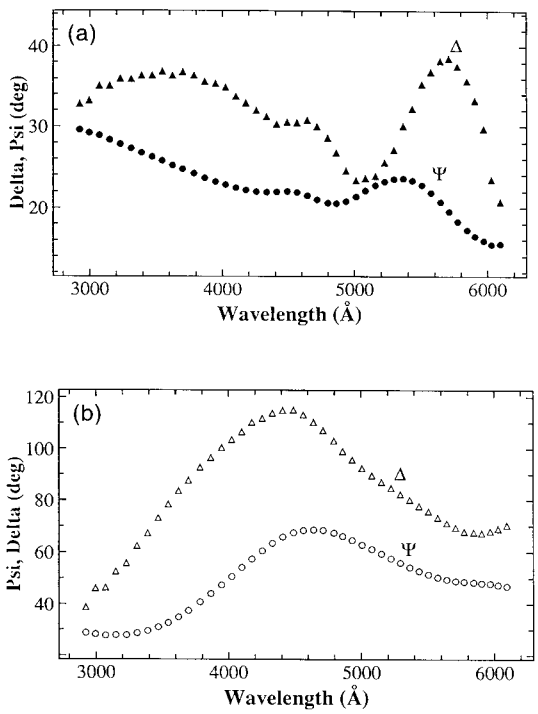

Fig. 5. Ellipsometric spectral parameters. (A) freshly deposited $Li_2Mn_4O_9$ thin film, (B) after 4 days exposure to 1.0 M $LiPF_6$ in EC/DMC electrolyte.

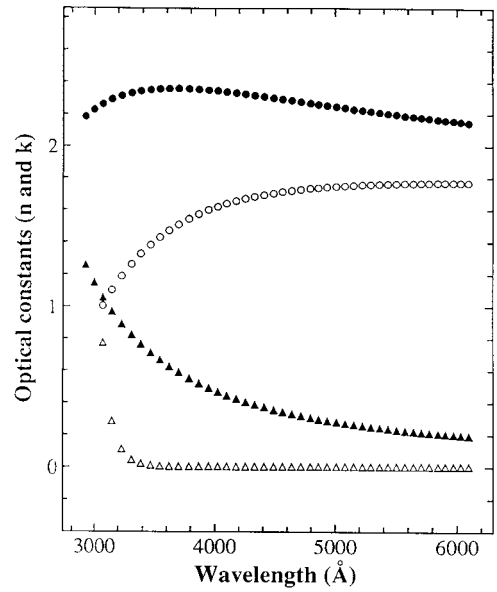

Fig. 6. Optical constants of a $Li_2Mn_4O_9$ thin film before and after exposure to electrolyte.

produce the very large changes of the tip-to-sample current as it is displayed in the image.

Figure 5(A) shows ellipsometric spectra of a freshly prepared film. The appearance of oscillations in the Δ, Ψ spectra indicates that the light beams reflected from both the upper and lower film surfaces ample interfered coherently. A two-layer model, i.e. a compact film overlaid with a porous layer (consisting of the active material and void spaces) provided good fit to the experimental data. Film roughness parameters were determined from AFM images and used in the fitting process.

Our prior studies [19] revealed that lithiated manganese oxide is not a strongly dispersive medium, and exhibits no sharp absorption peak over the visible spectrum. The optical behavior of a medium like $LiMn_2O_4$ can be represented by the so-called Cauchy dispersion model:

$$n(\lambda) = A + B/\lambda^2 + C/\lambda^4 \quad (1)$$

$$k(\lambda) = \alpha \exp\{\beta[12400(1/\lambda - 1/\gamma)]\} \quad (2)$$

where A, B and C are the zero-order and higher-order refractive indices respectively, α is the extinction coefficient amplitude, β is an exponential factor and γ is the band edge. In this case, 9 adjustable parameters (6 variables for the Cauchy dispersion model, the thickness of each layer and the volume fraction of void space in the porous layer) are required to describe our thin-film electrode. Even though this detailed film model has been greatly simplified by AFM measurement results, the practical data-fitting process remains complicated. We selected the zero-order refractive index and extinction coefficient amplitude as the first variables to determine (while fixing the remaining parameters) by iteration. Followed the same principle, we then adjusted the trial values for the remaining variables to arrive at a consistent solution set.

Optical constants of the thin-film electrode material which provided the best fit of the above described model to the experimental data are shown in Fig. 6. These values are very close to those for stoichiometric $LiMn_2O_4$ obtained from ellipsometric measurements of a powder pressed into a pellet and then polished to a mirror-like finish. A relatively high refractive index (n greater than 2 over most of the visible spectrum) and a moderate value of the extinction coefficient k is characteristic of an optically compact film of a semiconductor material. The calculated thicknesses are 422.5 and 25 nm for the compact film and porous overlayer, respectively, where the porous overlayer consists of 50/50 vol% film material and void space.

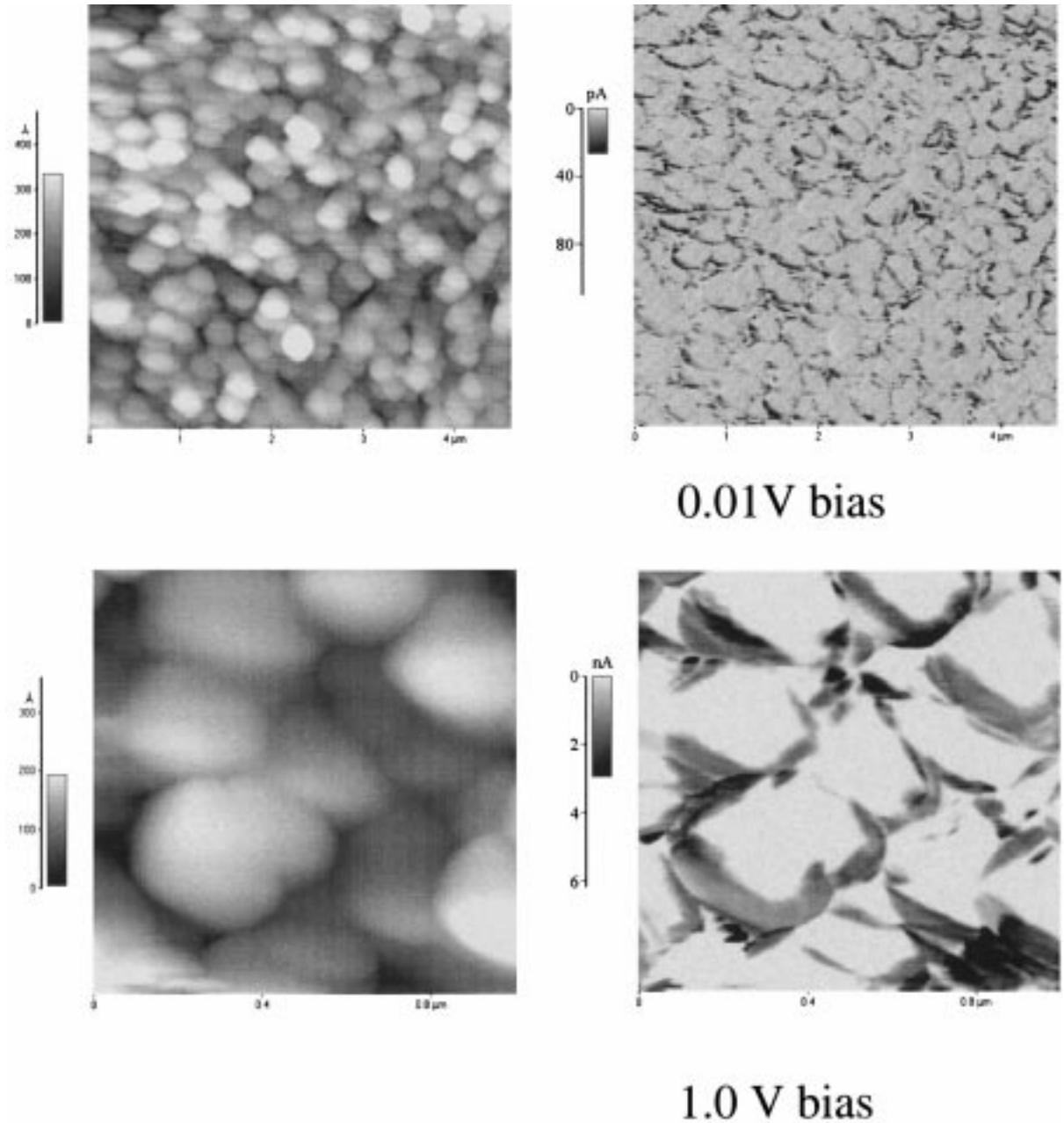

Fig. 7. CSAFM topographic (left) and conductivity (right) images of the thin-film electrode after 4 days exposure to 1.0 M $LiPF_6$ in EC/DMC electrolyte.

3.2. Interfacial studies of the active material thin film after exposure to the electrolyte

The thin-film $Li_2Mn_4O_9$ electrode was studied to detect possible changes in surface composition, structure and morphology upon exposure to 1.0 M $LiPF_6$-EC/DMC (1:1 by volume) electrolyte at room temperature. The electrode was held in the electrolyte at open circuit (~3.72 V) for 4 days, then it was soaked in pure DMC for 2 h to wash any residual salt from the film. The dry electrode was inserted into the ellipsometric cell in a He-atmosphere glove box and then transferred to the ellipsometer. A similar procedure was used for Raman measurements. CSAFM imaging was con-

ducted in a small glove box specially designed for scanning probe microscopy tests under a controlled He atmosphere.

Figure 1(B) shows the diffraction pattern of the thin-film material after 4 days exposure to the electrolyte at ambient temperature. It has much the same pattern, in terms of relative line positions, as the original $Li_2Mn_4O_9$ material but the lines are shifted to slightly higher angles and the peak intensity ratio changed noticeably. Thus, similar to the precursor oxide, this material could be indexed to a cubic unit cell, with lattice constant $a = 0.809$ nm.

The Raman spectrum of the electrolyte-exposed film is shown in Fig. 3(B) and exhibits even more drastic changes. The most prominent feature in this spectrum is the peak at 580 cm^{-1} which remained, while the peaks at 620 and 695 cm^{-1} almost disappeared (however, they contribute to the 580 cm^{-1} peak tail which extends to the high-frequency region of the spectrum). Usually, delithiation of $Li_xMn_{2-x}O_4$ leads to only slight variations of the vibrational spectra, suggesting that both the structure symmetry and atom occupancy undergo minor modifications. The spectrum of the thin film after exposure to electrolyte at room temperature is nearly identical to that of λ-MnO_2 [24]. To fully confirm the identity of this material, we fabricated a sample of λ-MnO_2 following the procedure described by Hunter [13]. The Raman spectrum of the reference sample was identical to the spectrum of the present sample after exposure to the electrolyte. The peak intensity ratio variation of the X-ray pattern [Fig. 1(B)] supports this conclusion. It appears that prolonged contact of the thin-film $Li_2Mn_4O_9$ electrode with 1.0 M $LiPF_6$ in EC/DMC electrolyte leads to formation of a manganese dioxide structure, derived from the cubic spinel structure of $LiMn_2O_4$ but with most of the lithium removed from the tetrahedral sites.

It is well documented that treatment of spinel-type $LiMn_2O_4$ with aqueous acid results in conversion of the precursor $LiMn_2O_4$ to nearly pure MnO_2, while preserving the structural framework of a cubic spinel [13]. Water traces present in the electrolyte will react with $LiPF_6$ to form HF which may promote the Li extraction process, albeit at a much slower rate. On the other hand, it was reported that manganese spinels undergo structural modifications when stored in a 1.0 M $LiPF_6$, EC:DMC (1:2 by volume) electrolyte, especially at elevated temperatures [25], but the authors suggested that Mn dissolution cause crystal lattice disorder. Pasquier et al. [16] proposed an aging scenario of $LiMn_2O_4$ whereby formation of a deficient spinel phase $Li_{1+2y}Mn_{2-y}O_4$ in acidic media is followed by ion exchange of H^+ and Li^+ and the formation of protonated λ-MnO_2 where protons are bonded to the oxygen atoms coordinating the 16d Mn vacancies. However, the Raman spectra of our films showed no bands characteristic of the OH group at ca. 3500 cm^{-1}. Thus, in the absence of any electrochemical process we can propose the following simple reaction scheme:

$$Li_2Mn_4O_9 \rightarrow 4\lambda - MnO_2 + Li_2O \quad (3)$$

A high concentration of point defects and significant crystal disorder in the original active material, as confirmed by the X-ray and Raman spectra, will certainly promote the lithium extraction process via disproportionation of Mn^{3+} impurities and the ion-exchange mechanism proposed in [13,16]. On the other hand we postulate that a poorly crystallized defect spinel undergoes spontaneous structural rearrangement in contact with 1.0 M $LiPF_6$, EC:DMC (1:1 by volume) electrolyte at room temperature, which involves the formation of separate regions of the λ-MnO_2 phase and most likely Li_2O. However, we cannot provide convincing spectral evidence for Li_2O at this time.

Examination of the topographic AFM images (Fig. 7) of the active material recorded after exposure to the electrolyte reveals no significant change in the film morphology. The initial globular structure was well preserved with no evidence of deposits, material corrosion or mechanical breakdown of the film. Consistent with the spectral data, Li was extracted from the $Li_2Mn_4O_9$ particles without significantly disrupting the structure of the precursor material and visibly changing the film morphology. It is difficult to determine at this stage if the entire film was converted. The calculated lattice constant is slightly higher than that reported in the literature [13] for a pure λ-MnO_2 phase ($a = 8.030$ Å), suggesting that the conversion was incomplete. On the other hand, the Raman spectra show the fingerprint of a basically pure λ-MnO_2 phase, however the Raman sensing depth is limited to that of light penetration, which is ca. 30 nm in this case.

Another clear signature of interfacial processes is provided by CSAFM images of the $Li_2Mn_4O_9$ film exposed to electrolyte. The conductivity dropped significantly over most of the film surface. The bright areas in the conductivity images exhibit no electronic conductivity within measurable limits. However, there remain small domains located mostly at the grain sides or grain boundaries which show conductivities comparable to the fresh film. Taking into account that λ-MnO_2 is a good electronic conductor, the observed changes in the film surface conductivity may be attributed to passive film formation, most likely composed of Li_2O. It has been already suggested that delithiated manganese oxide spinels may react with electrolyte, leading to passivation of the active material [16,26], the nature of which depends strongly on temperature and the Li salt used. Because we did not observe bands characteristic of an organic layer surrounding

the active material particles or bands specific for LiOH or Li_2CO_3, we suggest that the thin passive layer consists mainly of Li_2O which is insoluble in EC:DMC solvent. Another explanation of the loss of surface conductivity is the extensive structural disorder very close to the interface, induced by diffusing Li ions.

The ellipsometric parameters [shown in Fig. 5(B)] of the film exposed to the electrolyte also exhibit a dramatic change. Both Δ and Ψ are shifted to higher angles and display different spectral characteristics. We tried to use a similar two-layer model to fit the experimental data and calculate the optical constants and thickness of the film. However, this procedure did not work as well as it did for a fresh film, suggesting that the film underwent significant modifications and requires the use of additional parameters for a detailed description. We could, however, demonstrate that the film thickness decreased by ~40% and both n and k decreased (Fig. 6). A thinner film may be a result of partial delamination of sublayers which constitute the spin-coated film. Lower n and k values suggest a contribution from an insulating medium present at the film surface.

4. Conclusions

Lithium manganese oxide films were prepared by spin coating of a homogeneous precursor solution onto a Pt substrate. The coatings exhibited a defected spinel of stoichiometry close to $Li_2Mn_4O_9$. The film was electrochemically active and displayed capacity in both the 3 and 4 V regions. However, prolonged exposure of the film to 1.0 M $LiPF_6$, EC:DMC (1:1 by volume) electrolyte at room temperature resulted in spontaneous decomposition of the precursor material to λ-MnO_2 without disruption of the original spinel structure. Optical constants of the precursor film and the electrolyte-exposed film were determined from ellipsometric measurements. The surface of the resulting λ-MnO_2 film exhibited no significant change in morphology, however long exposure of the film to the electrolyte led to the formation of a thin insulating passive layer which was detected by the CSAFM probe and ellipsometry. A simple reaction scheme of the $Li_2Mn_4O_9$ conversion to λ-MnO_2 accompanied by the Li_2O extraction from the bulk of the film was proposed. The SEI layer has inorganic character and most likely consist of Li_2O.

Acknowledgements

This work was supported by the Assistant Secretary for Energy Efficiency and Renewable Energy, Office of Transportation Technologies, Office of Advanced Automotive Technologies of the US Department of Energy under Contract No. DE-AC03-76SF00098.

References

[1] P. Arora, R.E. White, M. Doyle, J. Electrochem. Soc. 145 (1998) 3647.
[2] J.M. Tarascon, D. Guyomard, J. Electrochem. Soc. 138 (1991) 2865.
[3] D. Aurbach, Y. Ein-Eli, O. Chusid, Y. Carmeli, M. Babai, H. Yamin, J. Electrochem. Soc. 141 (1994) 603.
[4] D. Aurbach, M.L. Daroux, P.W. Faguy, E. Yeager, J. Electrochem. Soc. 134 (1987) 1611.
[5] E. Peled, The Electrochemical Society Meeting Abstracts, vol. 94-2, Miami Beach, FL, Oct 9–14, Abstract 72, 1994, p. 114.
[6] E. Peled, D. Golodnitsky, G. Ardel, V. Eshkenazy, Electrochim. Acta 40 (1995) 2197.
[7] M.M. Thackeray, J. Electrochem. Soc. 142 (1995) 2558.
[8] J.M. Tarascon, W.R. McKinnon, F. Coowar, T.N. Bowmer, G. Amatucci, D. Guyomard, J. Electrochem. Soc. 141 (1994) 1421.
[9] G.G. Amatucci, J.M. Tarascon, L.C. Klien, Solid State Ionics 83 (1996) 167.
[10] S. Tobishima, K. Hayashi, K. Saito, T. Shodai, J. Yamaki, Electrochim. Acta 42 (1997) 119.
[11] A. Blyr, C. Sigala, G. Amatucci, D. Guyomard, Y. Chabre, J.M. Tarascon, J. Electrochem. Soc. 145 (1998) 194.
[12] O. Schilling, J.R. Dahn, J. Electrochem. Soc. 145 (1998) 569.
[13] J.C. Hunter, J. Solid State Chem. 39 (1981) 142.
[14] D.H. Jang, S.M. Oh, J. Electrochem. Soc. 144 (1997) 3342.
[15] Y. Xia, Y. Zhou, M. Yoshio, J. Electrochem. Soc. 144 (1997) 2593.
[16] A. Du Pasquier, A. Blyr, P. Courjal, D. Larcher, G. Amatucci, B. Gerand, J.-M. Tarascon, J. Electrochem. Soc. 146 (1999) 428.
[17] L.M.M. de Souza, F.P. Kong, F.R. McLarnon, R.H. Muller, Electrochim. Acta 42 (1997) 1253.
[18] F. Kong, R. Kostecki, F. McLarnon, J. Electrochem. Soc. 145 (1998) 1174.
[19] A. Rougier, F. Kong, R. Kostecki, K.A. Striebel, F. McLarnon and E.J. Cairns, Abstracts of the MRS Meeting, 1998, p. 396.
[20] F. Kong, J. Kim, X. Song, M. Inaba, K. Kinoshita, F. McLarnon, Electrochem. Solid-State Lett. 1 (1998) 39.
[21] K. Amine, H. Tsukamoto, H. Yasuda, Y. Fujita, The Electrochemical Society Meeting Abstracts, vol. 95-2, Chicago, Oct 8–16, Abstract 71, 1995, p. 157.
[22] P. Barboux, J.M. Tarascon, F.K. Shokoohi, J. Solid State Chem. 94 (1991) 185.
[23] A. de Kock, M.H. Rossouw, L.A. Picciotto, M. Thackeray, W.I.F. David, R.M. Ibberson, Mater. Res. Bull. 25 (1990) 657.
[24] H. Kanoh, W. Tang, K. Ooi, Electrochem. Solid Lett. 1 (1998) 17.
[25] T. Inoue, M. Sano, J. Electrochem. Soc. 145 (1998) 3704.
[26] Y. Gao, J.R. Dahn, Solid State Ionics 84 (1996) 33.